Optics Communications 389 (2017) 203–211

Contents lists available at ScienceDirect

Optics Communications

journal homepage: www.elsevier.com/locate/optcom

Diffraction of a Gaussian beam by a four-sector binary grating with a shift between adjacent sectors

Lj. Janicijevic[a], S. Topuzoski[a,*], L. Stoyanov[b], A. Dreischuh[b]

[a] Faculty of Natural Sciences and Mathematics, Institute of Physics, University "Ss. Cyril and Methodius", Skopje 1000, Republic of Macedonia
[b] Department of Quantum Electronics, Faculty of Physics, Sofia University "St. Kliment Ohridski", Sofia 1164, Bulgaria

ARTICLE INFO

Keywords:
Diffraction
Diffractive optical element
Gaussian laser beam
Four-sector binary grating

ABSTRACT

In this article as a diffractive optical element we consider a composed four-sector binary grating under Gaussian laser beam illumination. The angular sectors are bounded by the directions $y = x$ and $y = -x$, and consist of parts of a binary rectilinear grating; thereby, two neighboring parts are shifted by a half spatial rectilinear grating period. The diffracted wave field amplitude is calculated, showing that the straight-through, zeroth-diffraction-order beam is an amplitude-reduced Gaussian beam, and the higher-diffraction-order beams, deviated with respect to the propagation axis, are non-vortex beams described by modified Bessel functions. The transverse intensity profiles of the higher-diffraction-order beams, numerically and experimentally obtained, have form of a four-leaf clover; they are similar to the Laguerre-Gaussian LG(0,2) beam (with radial mode number $n = 0$ and azimuthal mode number $l = 2$) described by circular cosine function, in a paraxial, far-field approximation.

1. Introduction

Besides the fundamental mode (Gaussian beam), the Hermite–Gaussian (HG) and Laguerre–Gaussian (LG) beams are also solutions of the paraxial wave equation [1]. Lot of research has been done to analyze their theoretical and experimental properties, and to investigate their applications in the basic optical sciences and in other scientific fields (see e.g. Ref. 2 and references therein). Linearly polarized LG beams with nonzero azimuthal mode number are carriers of screw dislocations and possess orbital angular momentum (OAM) [3]. They are optical vortex beams. In the field of singular optics the mostly used are LG beams with zero radial mode number. The family of LG beams covers the cases of the equiaxial linear combinations (addition or subtraction) of two LG beams with equal azimuthal mode number value l, but with opposite signs of l (opposite orientations of their OAMs), as well. As a result, the two coupled vortex beams create a beam without OAM (no topological charge), possessing profiles described by circular functions $\cos(l\varphi)$ or $\sin(l\varphi)$.

The linearly polarized HG(m,n) beams have degenerate edge dislocations in their wavefronts and do not possess OAM [3].

Nye and Berry have described, classified and analyzed the wavefronts defects in wave trains and monochromatic waves [4]. In laser beams having structure of transverse cavity modes, edge dislocations occur as black lines between π-shifted in phase mode spots; the simplest is the TEM_{01}, where the zeroth-value intensity line divides the beam into two parts corresponding to phase shift of π. In [5] the authors showed that, an edge dislocation of the wavefront can be produced experimentally by using two binary periodic gratings, shifted by half a period on a line of zero amplitude. Then, in the process of diffraction, the incident Gaussian laser beam is divided with a dark line into two bright spots. Whereas, a binary fork-shaped grating with an edge dislocation in direction $\theta = 0$ produces mixed screw-edge dislocation, as shown experimentally in [5].

The vortex beams are created in laser resonators, or by using diffractive optical elements which transform the Gaussian beam into a vortex one, such as spiral phase plate [6–8], helical axicon [9–12], helical lens [13], computer-generated holograms [14,15], fork-shaped gratings [16,17] etc. The computer-generated gratings (CGGs) accompanied with the photo-reduction methods have an advantage over the expensive lithographic methods. Except the simple, fast and cheap production, they make possible the creation of combined gratings, which can substitute the laser resonators in making new interesting laser modes. Liquid crystal spatial light modulators make this procedure even more flexible ensuring high efficiency and fast reconfiguration.

In this article we consider a CGG constructed by inserting parts of a binary rectilinear grating into the four equal angular sectors, bounded by the directions $y = x$ and $y = -x$ (Fig. 1). Thus, two neighboring parts

* Corresponding author.
E-mail address: suzana_topuzoski@yahoo.com (S. Topuzoski).

http://dx.doi.org/10.1016/j.optcom.2016.12.041
Received 20 November 2016; Received in revised form 14 December 2016; Accepted 18 December 2016
Available online 27 December 2016

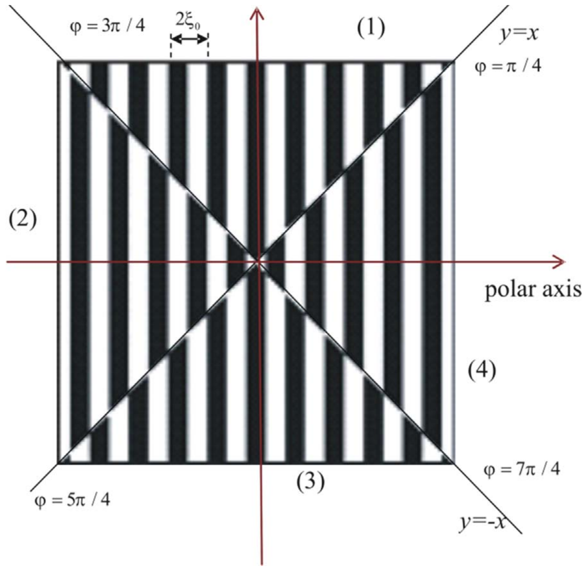

Fig. 1. The computer-generated four-sector grating.

of the grating are shifted by a half spatial grating period along x axis. We analytically calculate the diffraction pattern obtained by illuminating the grating with a Gaussian laser beam, which enters into the grating plane with its waist and intersects the grating plane centre with its axis. The far-field diffraction patterns of the higher-diffraction-order (HDO) beams, in a paraxial approximation are similar to Hermite-Gaussian HG(1,1) or cosine-LG(n=0,l=2) laser mode: four bright spots are nested in four quadrants divided by crossed one-dimensional phase dislocations. With this method we create in the HDOs beams with coupled optical vortices [18] and crossed dark lines, which are of interest for many applications as optical trapping, optical communication, angular alignment etc.

2. Construction and transmission function of the grating

The computer generation of this grating consists in inserting parts of a binary rectilinear grating into the four equal angular sectors, bounded by the directions $y = x$ and $y = -x$. The area of each of the sectors, numbered by n=(1), (2), (3) and (4), is successively covered by a negative (in (1) and (3)) and positive (in (2) and (4)) gratings, both possessing the same period $d = 2\xi_0$ (Fig. 1). In a rectangular coordinate system, whose ordinate is the axis of symmetry of both types of gratings, their transmission functions are expressed by the cosine Fourier series as

$$t_g^{\pm}(x) = \frac{1}{2} \pm \sum_{m=1}^{\infty} \mathrm{sinc}\left((2m-1)\frac{\pi}{2}\right)\cos\left((2m-1)\frac{\pi}{\xi_0}x\right). \tag{1}$$

Since we will treat the problem of diffraction of a Gaussian laser beam by the computer-generated gratings in cylindrical coordinate system, we will use the polar coordinates (r, φ) for the grating's plane. The pole is situated in the intersection point of the $y = x$ and $y = -x$ lines. Then, the transmission functions $t_g^{+}(r, \varphi)$ for the positive (with white central line) and $t_g^{-}(r, \varphi)$ for the negative (with dark central line) gratings, are defined as

$$t_g^{\pm}(r, \varphi) = \frac{1}{2} \pm \frac{1}{2}\sum_{m=1}^{\infty} \mathrm{sinc}\left((2m-1)\frac{\pi}{2}\right)\left[\exp\left(+i(2m-1)\frac{\pi}{\xi_0}r\cos\varphi\right) + \exp\left(-i(2m-1)\frac{\pi}{\xi_0}r\cos\varphi\right)\right]. \tag{2}$$

In Eq. (1) and Eq. (2) the transmission coefficients are $\mathrm{sinc}((2m-1)\pi/2) = 2(-1)^{(m-1)}/(\pi(2m-1))(m = 1, 2, 3, \ldots)$, while the sign "+" in front of the sum stands for the positive grating.

As it is seen in Fig. 1, the n-th quadrant is occupied by one of the upper mentioned gratings. Each of them is an angular sector of π/2 rad, which in absence of the grating, is a completely transparent aperture between the directions $\varphi = (2n-1)\pi/4$ and $\varphi = (2n+1)\pi/4$. Using the Heaviside unite step function $E(\varphi - \varphi_0) = \begin{cases} 1 & \varphi > \varphi_0 \\ 0 & \text{otherwise} \end{cases} \ (0 < \varphi < 2\pi)$, we define the n-th sector aperture transmission function as

$$t_a^{(n)}(\varphi) = E(\varphi - (2n-1)\pi/4) - E(\varphi - (2n+1)\pi/4) = \begin{cases} 1 & (2n-1)\pi/4 < \varphi < (2n+1)\pi/4 \\ 0 & \text{otherwise} \end{cases} \quad (n = 1, 2, 3, 4) \tag{3}$$

The transmission function of the composed grating in Fig. 1 is a sum of the four sector transmission functions $t(r, \varphi) = t_a^{(n)}(\varphi)t_g^{\pm}(r, \varphi)$ (for n=1,2,3,4) and is defined by

$$t(r, \varphi) = \sum_{n=1}^{4}\{E(\varphi - (2n-1)\pi/4) - E(\varphi - (2n+1)\pi/4)\} \times \left\{\frac{1}{2} + (-1)^n\sum_{m=1}^{\infty}\mathrm{sinc}\left((2m-1)\frac{\pi}{2}\right)\cos\left((2m-1)\frac{\pi}{\xi_0}r\cos\varphi\right)\right\}. \tag{4}$$

The grating whose transmission function is given by expression Eq. (4) will be used as an optical diffracting device in our further investigation.

3. Diffraction of a Gaussian laser beam by the composed four-sector grating

The Gaussian beam is normally incident on the plane of the grating, with its propagation axis (z axis of the cylindrical coordinate system) passing through its centre, and its waist located in the plane of the grating. Thus, the incident beam is defined by: $U^i(r, \varphi, z = 0) = \exp(-r^2/w_0^2) = \exp(-ikr^2/2q(0))$ where w_0 is the beam waist radius, $k = 2\pi/\lambda$ is the propagation constant and $q(0)$ is the beam complex parameter in the waist plane. If the grating is absent, at distance z from the origin the beam has a complex parameter $q(z) = z + ikw_0^2/2$, with $q(0) = ikw_0^2/2 = iz_0$, and z_0 being the beam Rayleigh distance. The field of the diffracted light is defined by the Fresnel-Kirchhoff integral

$$U(\rho, \theta, z) = \frac{ik}{2\pi z}\exp\left[-ik\left(z + \frac{\rho^2}{2z}\right)\right]\int_0^{\infty}\int_0^{2\pi} t(r, \varphi)U^{(i)}(r, \varphi) \times \exp\left[-\frac{ik}{2z}(r^2 - 2r\rho\cos(\varphi - \theta))\right] r\,\mathrm{d}r\,\mathrm{d}\varphi. \tag{5}$$

The polar coordinates (ρ, θ) characterize the observation plane Π situated at distance z from the grating. Substitution of the incident beam and the transmission function Eq. (4) in the diffraction integral gives

$$U(\rho, \theta, z) = \sum_{n=1}^{4}\left[U_{m=0}(\rho, \theta, z) + \sum_{m=1}^{\infty}(U_{+(2m-1)}(\rho, \theta, z) + U_{-(2m-1)}(\rho, \theta, z))\right]. \tag{6}$$

The part of the solution $\sum_{n=1}^{4} U_{m=0}(\rho, \theta, z)$ defines the zeroth diffraction order

$$U_{m=0}(\rho,\theta,z)=\frac{ik}{4\pi z}\exp\left[-ik\left(z+\frac{\rho^2}{2z}\right)\right]\int_0^\infty\left\{\exp\left(-\frac{ik}{2z}\frac{q(z)}{q(0)}r^2\right)\right.\\ \times\sum_{n=1}^{4}\int_0^{2\pi}[E(\varphi-(2n-1)\pi/4)\\ -E(\varphi-(2n+1)\pi/4)]\\ \left.\times\exp\left[\frac{ik\rho r}{z}\cos(\varphi-\theta)\right]\mathrm{d}\varphi\right\}r\mathrm{d}r. \tag{7}$$

Considering that $\int_0^{2\pi}[E(\varphi-(2n-1)\pi/4)-E(\varphi-(2n+1)\pi/4)]F'(\varphi)\mathrm{d}\varphi=\int_{(2n-1)\frac{\pi}{4}}^{(2n+1)\frac{\pi}{4}}F'(\varphi)\mathrm{d}\varphi$, and using the integral representation of the Bessel functions (Eq. 9.1.21 in [19]): $J_\nu(\alpha)=(i^{-\nu}/\pi)\int_0^\pi\exp(i\alpha\cos\beta)\cos(\nu\beta)\mathrm{d}\beta$ for the solution $\int_0^{2\pi}\exp\left[\frac{ik\rho}{z}r\cos(\varphi-\theta)\right]\mathrm{d}\varphi=2\pi J_0\left(\frac{k\rho}{z}r\right)$, we end up with the expression

$$U_{m=0}(\rho,\theta,z)=\frac{ik}{2z}\exp\left[-ik\left(z+\frac{\rho^2}{2z}\right)\right]\int_0^\infty J_0\left(\frac{k\rho}{z}r\right)\exp\left[-\frac{ik}{2z}\frac{q(z)}{q(0)}r^2\right]r\mathrm{d}r. \tag{8}$$

To carry out the integration over the radial variable, the referent integral Eq. 11.4.29 in [19] is used. After replacing its solution in Eq. (8), we get the zeroth-diffraction-order wave amplitude in the form

$$U_{m=0}(\rho,\theta,z)=\frac{1}{2}\frac{q(0)}{q(z)}\exp\left[-ik\left(z+\frac{\rho^2}{2q(z)}\right)\right]. \tag{9}$$

It represents the incident Gaussian beam at distance z from its waist, being amplitude reduced by 1/2.

The field of the higher diffraction orders is represented by the second part of expression Eq. (6)

$$\sum_{n=1}^{4}\sum_{m=1}^{\infty}(U_{+(2m-1)}(\rho,\theta,z)+U_{-(2m-1)}(\rho,\theta,z))=\frac{ik}{4\pi z}\exp\left[-ik\left(z+\frac{\rho^2}{2z}\right)\right]\\ \times\sum_{m=1}^{\infty}\mathrm{sinc}\left((2m-1)\frac{\pi}{2}\right)\\ \times\int_0^\infty\left\{\exp\left[\frac{-ik}{2z}\frac{q(z)}{q(0)}r^2\right]\sum_{n=1}^{4}(-1)^n\int_0^{2\pi}\left\{E\left[\varphi-(2n-1)\frac{\pi}{4}\right]\right.\right.\\ \left.-E\left[\varphi-(2n+1)\frac{\pi}{4}\right]\right\}\exp\left[\frac{ik\rho}{z}r\cos(\varphi-\theta)\right]\\ \left.\times\left\{\exp\left[i(2m-1)\frac{\pi}{\xi_0}r\cos\varphi\right]+\exp\left[-i(2m-1)\frac{\pi}{\xi_0}r\cos\varphi\right]\right\}\mathrm{d}\varphi\right\}r\mathrm{d}r. \tag{10}$$

Before we start performing the integration over the azimuthal variable, we will do an rearrangement of the exponents with the variable φ in Eq. (10). By introducing a shorter notation

$$x_0=\lambda z/(2\xi_0) \tag{11}$$

we can write the exponents containing the diffraction orders $(2m-1)$ as

$$\exp[\pm i(2m-1)(\pi/\xi_0)r\cos\varphi]=\exp[\pm i(2m-1)(kx_0/z)r\cos\varphi]. \tag{12}$$

For each HDO $(2m-1)$, new variables $\rho_{\pm(2m-1)}$ and $\theta_{\pm(2m-1)}$ are defined in the following way

$$\rho\cos\theta\pm(2m-1)x_0=\rho_{\pm(2m-1)}\cos\theta_{\pm(2m-1)}\text{ and }\rho\sin\theta=\rho_{\pm(2m-1)}\sin\theta_{\pm(2m-1)}$$

where

$$\rho_{\pm(2m-1)}=\sqrt{\rho^2\pm2(2m-1)x_0\rho\cos\theta+(2m-1)^2x_0^2}\text{ and }\theta_{\pm(2m-1)}=\arctan\left(\frac{\rho\sin\theta}{\rho\cos\theta\pm(2m-1)x_0}\right), \tag{13}$$

and the opposite relations (expressing coordinates ρ and θ through $\rho_{\pm(2m-1)}$ and $\theta_{\pm(2m-1)}$) are

$$\rho=\sqrt{\rho_{\pm(2m-1)}^2\mp2(2m-1)x_0\rho_{\pm(2m-1)}\cos\theta_{\pm(2m-1)}+(2m-1)^2x_0^2},\text{ and}\\ \theta=\arctan\left(\frac{\rho_{\pm(2m-1)}\sin\theta_{\pm(2m-1)}}{\rho_{\pm(2m-1)}\cos\theta_{\pm(2m-1)}\mp(2m-1)x_0}\right). \tag{13a}$$

These new local variables Eq. (13) are associated to coordinate systems whose roots in the observation plane $\Pi(\rho,\theta)$ are located at directions $\theta=\pi$ and $\theta=0$ (for negative and positive HDOs, respectively), at points $O_{(2m-1)}(\rho=(2m-1)x_0,\theta=\pi)$ and $O_{-(2m-1)}(\rho=(2m-1)x_0,\theta=0)$. Two neighboring roots are found at a distance $\overline{O_{2m+1}O_{2m-1}}=2x_0=\lambda z/\xi_0$ from each other. The $(2m-1)$-th diffraction order consists of two components deviated at angle $\delta_{\pm(2m-1)}=\arctan((2m-1)\lambda/(2\xi_0))$. Now, the higher $(2m-1)$-th diffraction order is defined by

$$U_{+(2m-1)}+U_{-(2m-1)}=\frac{ik}{4\pi z}\exp\left[-ik\left(z+\frac{\rho^2}{2z}\right)\right]\mathrm{sinc}\left[(2m-1)\frac{\pi}{2}\right]\\ \times\int_0^\infty\left\{\exp\left[\frac{-ik}{2z}\frac{q(z)}{q(0)}r^2\right]\right.\\ \times[\Theta_{+(2m-1)}(\rho_{+(2m-1)},\theta_{+(2m-1)},z)\\ \left.+\Theta_{-(2m-1)}(\rho_{-(2m-1)},\theta_{-(2m-1)},z)]\right\}r\mathrm{d}r \tag{14}$$

where, according to Eq. (10)

$$\Theta_{\pm(2m-1)}(\rho_{\pm(2m-1)},\theta_{\pm(2m-1)},z)\\ =\sum_{n=1}^4(-1)^n\int_{(2n-1)\pi/4}^{(2n+1)\pi/4}\exp\left[\frac{ik\rho_{\pm(2m-1)}}{z}r\cos(\varphi-\theta_{\pm(2m-1)})\right]\mathrm{d}\varphi\\ =J_0\left(\frac{k\rho_{\pm(2m-1)}}{z}r\right)\sum_{n=1}^4(-1)^n\int_{(2n-1)\pi/4}^{(2n+1)\pi/4}\mathrm{d}\varphi\\ +2\sum_{j=1}^\infty\left\{i^jJ_j\left(\frac{k\rho_{\pm(2m-1)}}{z}r\right)\sum_{n=1}^4(-1)^n\right.\\ \left.\times\int_{(2n-1)\pi/4}^{(2n+1)\pi/4}\cos[j(\varphi-\theta_{\pm(2m-1)})]\mathrm{d}\varphi\right\}. \tag{15}$$

In Eq. (15) the Jacoby-Anger identity [20] for the Bessel functions: $\exp(iz\cos\theta)=\sum_{s=-\infty}^{\infty}i^s\exp(is\theta)J_s(z)$

is used. The summation done on the solutions of the two integrals over the azimuthal variable gives the following results

$$\sum_{n=1}^4(-1)^n\int_{(2n-1)\pi/4}^{(2n+1)\pi/4}\mathrm{d}\varphi=\frac{\pi}{2}\sum_{n=1}^4(-1)^n=0 \tag{16a}$$

and

$$\sum_{n=1}^4(-1)^n\int_{(2n-1)\pi/4}^{(2n+1)\pi/4}\cos[j(\varphi-\theta_{\pm(2m-1)})]\mathrm{d}\varphi\\ =\frac{2}{j}\sin\left(j\frac{\pi}{4}\right)\times\sum_{n=1}^4(-1)^n\cos\left[\frac{j}{2}(n\pi-2\theta_{\pm(2m-1)})\right]\\ =\begin{cases}\frac{8(-1)^{l+1}}{2(2l-1)}\cos[2(2l-1)\theta_{\pm(2m-1)}] & \text{for}\quad j=2(2l-1)\\ 0 & \text{for other values of } j\end{cases} \tag{16b}$$

Therefore, introduction of

$$\Theta_{\pm(2m-1)}(\rho_{\pm(2m-1)},\theta_{\pm(2m-1)},z)=16\sum_{l=1}^\infty\frac{(-1)^l}{2(2l-1)}J_{2(2l-1)}\left(\frac{k\rho_{\pm(2m-1)}}{z}r\right)\\ \times\cos[2(2l-1)\theta_{\pm(2m-1)}] \tag{17}$$

in Eq. (14) yields

$$U_{+(2m-1)} + U_{-(2m-1)} = \frac{4ik}{\pi z}\exp\left[-ik\left(z + \frac{\rho^2}{2z}\right)\right]\mathrm{sinc}\left[(2m-1)\frac{\pi}{2}\right]\sum_{l=1}^{\infty}\frac{(-1)^l}{2(2l-1)} \times \{\cos[2(2l-1)\theta_{+(2m-1)}]Y_{+(2m-1)}(\rho_{+(2m-1)}, z) + \cos[2(2l-1)\theta_{-(2m-1)}]Y_{-(2m-1)}(\rho_{-(2m-1)}, z)\}. \tag{18}$$

In Eq. (18)$Y_{\pm(2m-1)}(\rho_{\pm(2m-1)}, z)$ are integrals over the radial variable i.e.

$$Y_{\pm(2m-1)}(\rho_{\pm(2m-1)}, z) = \int_0^{\infty}\exp\left[-\frac{ik}{2z}\frac{q(z)}{q(0)}r^2\right]J_{2(2l-1)}\left(\frac{k\rho_{\pm(2m-1)}}{z}r\right)r\mathrm{d}r \tag{19}$$

and they are of the same type as the reference integrals A_ν^2, Eq.2.12.9 (3) in [21]

$$A_\nu^2 = \int_0^{\infty} r^{2-1}\exp(-br^2)J_\nu(cr)\mathrm{d}r = \frac{c\sqrt{\pi}}{8b^{3/2}}\exp(-c^2/(8b)) [I_{(\nu-1)/2}(c^2/(8b)) - I_{(\nu+1)/2}(c^2/(8b))].$$

In our case $\nu = 2(2l-1)$, $c = k\rho_{\pm(2m-1)}/z$, $b = \frac{ik}{2}\frac{q(z)}{zq(0)}$ and $\frac{c^2}{8b} = \frac{k}{4i}\frac{q(0)}{zq(z)}\rho^2_{\pm(2m-1)}$. Thus

$$Y_{\pm(2m-1)}(\rho_{\pm(2m-1)}, z) = \frac{1}{4i}\frac{q(0)}{q(z)}\sqrt{\frac{\lambda}{i}\frac{zq(0)}{q(z)}}\rho_{\pm(2m-1)}\exp\left[\frac{ik}{4}\frac{q(0)}{zq(z)}\rho^2_{\pm(2m-1)}\right] \times\left[I_{(2(2l-1)-1)/2}\left(\frac{k}{4i}\frac{q(0)}{zq(z)}\rho^2_{\pm(2m-1)}\right) - I_{(2(2l-1)+1)/2}\left(\frac{k}{4i}\frac{q(0)}{zq(z)}\rho^2_{\pm(2m-1)}\right)\right] \tag{20}$$

while the branches of the $(2m-1)$-th diffraction orders are given by the expression

$$U_{\pm(2m-1)}(\rho_{\pm(2m-1)}, \theta_{\pm(2m-1)}, z) = \mathrm{sinc}\left[(2m-1)\frac{\pi}{2}\right]\frac{q(0)}{q(z)}\sqrt{\frac{2k}{i\pi}\frac{q(0)}{zq(z)}} \times\exp\left\{-ik\left[z + \frac{1}{2z}(\rho^2_{\pm(2m-1)} \mp 2(2m-1)x_0\rho_{\pm(2m-1)}\cos\theta_{\pm(2m-1)} + (2m-1)^2x_0^2)\right]\right\} \times\sum_{l=1}^{\infty}\frac{(-1)^l}{2(2l-1)}\cos[2(2l-1)\theta_{\pm(2m-1)}]\left\{\rho_{\pm(2m-1)}\exp\left[\frac{ik}{4}\frac{q(0)}{zq(z)}\rho^2_{\pm(2m-1)}\right] \times\left[I_{\frac{(2(2l-1)-1)}{2}}\left(\frac{k}{4i}\frac{q(0)}{zq(z)}\rho^2_{\pm(2m-1)}\right) - I_{\frac{(2(2l-1)+1)}{2}}\left(\frac{k}{4i}\frac{q(0)}{zq(z)}\rho^2_{\pm(2m-1)}\right)\right]\right\}. \tag{21}$$

If instead complex, we use the real parameters of the incident beam, the following replacements are needed:

$$\frac{q(0)}{q(z)} = \frac{w_0}{w(z)}\exp[i\arctan(z/z_0)];\quad \frac{1}{q(z)} = \frac{1}{R(z)} - \frac{2i}{kw^2(z)};$$
$$\frac{q(0)}{zq(z)} = \frac{1}{z} - \frac{1}{q(z)} = \left(\frac{1}{z} - \frac{1}{R(z)}\right) + \frac{2i}{kw^2(z)}$$

with $w(z) = w_0\sqrt{1 + (z/z_0)^2}$ and $R(z) = z(1 + (z_0/z)^2)$ being the radii of the transverse cross-section and of the beam wave front curvature. In that case: $\frac{ik}{4}\frac{q(0)}{zq(z)} = \left\{\frac{ik}{2}\frac{1}{2(z/z_0)^2R(z)} - \frac{1}{2w^2(z)}\right\}$.

Further we will denote

$$w'^2(z) = 2w^2(z) \text{ and } R'(z) = 2(z/z_0)^2R(z) = 2z[1 + (z/z_0)^2] = 2zw^2(z)/w_0^2 \tag{22}$$

and treat them as new real parameters of the $(2m-1)$-th diffraction order beam, since now: $\frac{k}{4i}\frac{q(0)}{zq(z)} = \frac{1}{w'^2(z)} - \frac{ik}{2R'(z)}$.

Considering that the wave field $U_{\pm(2m-1)}$ can be written by its amplitude $A_{\pm(2m-1)}$ and phase term $F_{\pm(2m-1)}$ as $U_{\pm(2m-1)} = A_{\pm(2m-1)}\exp(-iF_{\pm(2m-1)})$, it is not difficult to see that the amplitude profile function of the $(2m-1)$-th diffraction order beam Eq. (21) is

$$A_{\pm(2m-1)}(\rho_{\pm(2m-1)}, \theta_{\pm(2m-1)}, z) = 2\mathrm{sinc}\left[(2m-1)\frac{\pi}{2}\right]\frac{w_0'}{w'(z)}\sqrt{\left|\frac{2k}{i\pi}\left(\frac{2}{R'(z)} + \frac{4i}{kw'^2(z)}\right)\right|}\rho_{\pm(2m-1)}\exp\left(\frac{-\rho^2_{\pm(2m-1)}}{w'^2(z)}\right) \times\sum_{l=1}^{\infty}\frac{(-1)^l}{2(2l-1)}\cos[2(2l-1)\theta_{\pm(2m-1)}] \times\left|\left\{I_{(2l-1)-1/2}\left[\left(\frac{1}{w'^2(z)} - \frac{ik}{2R'(z)}\right)\rho^2_{\pm(2m-1)}\right] - I_{(2l-1)+1/2}\left[\left(\frac{1}{w'^2(z)} - \frac{ik}{2R'(z)}\right)\rho^2_{\pm(2m-1)}\right]\right\}\right|. \tag{23}$$

Due to the decreasing of the series coefficients $C_l = \left|\frac{(-1)^l}{2(2l-1)}\right| = \frac{1}{2}, \frac{1}{6}, \frac{1}{10}, \frac{1}{14}\ldots; l = 1, 2, 3, 4, \ldots$, it is possible to ignore series members with $l > 1$. We will demonstrate in the next section the effect of the presence of terms in the sum in Eq. (23) for l higher than 1, on the far-field diffraction patterns. In the approximation when taking into account only the term for $l = 1$, which will be used in our further investigation, the $(2m-1)$-th diffraction-order beam is defined by

$$U_{\pm(2m-1)}(\rho_{\pm(2m-1)}, \theta_{\pm(2m-1)}, z) = 2\mathrm{sinc}\left[(2m-1)\frac{\pi}{2}\right]\frac{w_0'}{w'(z)}\sqrt{\left|\frac{2k}{i\pi}\left(\frac{2}{R'(z)} + \frac{4i}{kw'^2(z)}\right)\right|}\rho_{\pm(2m-1)}\exp\left(\frac{-\rho^2_{\pm(2m-1)}}{w'^2(z)}\right) \times\cos(2\theta_{\pm(2m-1)})\left|\left\{I_{1/2}\left(\left(\frac{1}{w'^2(z)} - \frac{ik}{2R'(z)}\right)\rho^2_{\pm(2m-1)}\right) - I_{3/2}\left(\left(\frac{1}{w'^2(z)} - \frac{ik}{2R'(z)}\right)\rho^2_{\pm(2m-1)}\right)\right\}\right| \times\exp\left\{-ik\left\{z + \frac{1}{2z}\left[\left(1 - \frac{w_0'^2}{2w'^2(z)}\right)\rho^2_{\pm(2m-1)} \mp 2(2m-1)x_0\rho_{\pm(2m-1)}\cos\theta_{\pm(2m-1)} + (2m-1)^2x_0^2\right] - \frac{1}{k}\arctan\left(\frac{z}{z_0'}\right)^{3/2} - \frac{1}{k}\arctan\phi\right\}\right\} \tag{24}$$

where $\phi = \frac{\mathrm{Im}(I_{1/2}(\eta) - I_{3/2}(\eta))}{\mathrm{Re}(I_{1/2}(\eta) - I_{3/2}(\eta))}$ and $\eta = \left(\frac{1}{w'^2(z)} - \frac{ik}{2R'(z)}\right)\rho^2_{\pm(2m-1)}$.

The separate treatment of the beam is possible if it is undisturbed by interference with the neighboring diffraction-order beams. The condition to avoid interference is $\lambda z/\xi_0 > 2w_{beam}$ or $z > 2\xi_0 w_{beam}/\lambda$ where w_{beam} is the beam transverse cross-section dimension. That is the reason why when the diffraction objects are gratings (which produce many diffraction orders), the far-field investigation is preferable.

The authors in [22] in Section 4 of their article give a picture (Fig. 4b) of a CGG as a substitute to the fork-shaped grating. It is composed of four sectors, bounded by the lines $y = \pm x$, in which the rectilinear grating parts meet on the boundaries displaced by a rate $\xi_0/2$ (the quarter of the binary grating period). The displacements on the same boundaries, in the case of CGG (Fig. 1), treated in this article, is ξ_0 i.e. a half period of rectilinear grating. What are the consequences of the displacement difference, will be seen in the next section.

4. Discusion of the results in the far-field approximation

By neglecting the terms in the amplitude profile function $A_{\pm(2m-1)}$ which have $R'(z)$ and z in their denominator, and the small term $\rho^2_{\pm(2m-1)}/z$ in the phase function in Eq. (24), we get the so called far-field approximation of Eq. (24)

$$\begin{aligned}
U_{\pm(2m-1)}(\rho_{\pm(2m-1)},\theta_{\pm(2m-1)},z) &= \sqrt{\frac{8}{\pi}}\operatorname{sinc}\left[(2m-1)\frac{\pi}{2}\right]\\
&\times \exp\left\{-ik\left[z \mp \frac{(2m-1)x_0}{z}\rho_{\pm(2m-1)}\cos(\theta_{\pm(2m-1)}) + \frac{(2m-1)^2x_0^2}{2z}\right]\right\}\\
&\times \frac{w_0'}{w'(z)}\frac{\rho_{\pm(2m-1)}}{w'(z)}\exp\left[-\frac{\rho^2_{\pm(2m-1)}}{w'^2(z)}\right]\cos(2\theta_{\pm(2m-1)})\\
&\times \left\{I_{1/2}\left(\frac{\rho^2_{\pm(2m-1)}}{w'^2(z)}\right) - I_{3/2}\left(\frac{\rho^2_{\pm(2m-1)}}{w'^2(z)}\right)\right\}.
\end{aligned}\tag{25}$$

In both presentations of the beam field, Eq. (24) and Eq. (25), the parts which include variables $\rho_{\pm(2m-1)}$ and z, are similar in form with those representing the $(2m-1)$-th diffraction order of a binary fork-shaped grating with topological charge p (Eq. (30) in [16]). But, there are some essential differences. Let us compare solution (25) with the far-field approximation of the HDOs for the fork-shaped grating having TC p, given by

$$\begin{aligned}
U_{\pm(2m-1)}(\rho_{\pm(2m-1)},\theta_{\pm(2m-1)},z) &= \sqrt{\frac{8}{\pi}}\operatorname{sinc}\left[(2m-1)\frac{\pi}{2}\right]\\
&\times \exp\left\{-ik\left[z \mp \frac{(2m-1)x_0}{z}\rho_{\pm(2m-1)}\cos\theta_{\pm(2m-1)} + \frac{(2m-1)^2x_0^2}{2z}\right]\right\}\\
&\times \exp[\pm i(2m-1)p\theta_{\pm(2m-1)}]\frac{w_0'}{w'(z)}\frac{\rho_{\pm(2m-1)}}{w'(z)}\exp\left[-\frac{\rho^2_{\pm(2m-1)}}{w'^2(z)}\right]\\
&\times \left\{I_{((2m-1)p-1)/2}\left(\frac{\rho^2_{\pm(2m-1)}}{w'^2(z)}\right) - I_{((2m-1)p+1)/2}\left(\frac{\rho^2_{\pm(2m-1)}}{w'^2(z)}\right)\right\}.
\end{aligned}\tag{26}$$

The first difference is the existence of the circular function with azimuthal variable $\cos(2\theta_{\pm(2m-1)})$ as a part of the amplitude profile of expression (25). It modulates the amplitude function with its zero values. Since $\cos(2\theta_{\pm(2m-1)}) = (\cos\theta_{\pm(2m-1)} - \sin\theta_{\pm(2m-1)})(\cos\theta_{\pm(2m-1)} + \sin\theta_{\pm(2m-1)})$ it is clear that its zero values in the observation plane occur for values of $\theta_{\pm(2m-1)}$ (m=1,2,3...) which satisfy the equations

$$\begin{aligned}
&\begin{cases}\cos\theta_{\pm(2m-1)} - \sin\theta_{\pm(2m-1)} = 0\\ \text{or} \qquad \tan\theta_{\pm(2m-1)} = 1\end{cases} \qquad (a)\\
\text{and}\ &\begin{cases}\cos\theta_{\pm(2m-1)} + \sin\theta_{\pm(2m-1)} = 0\\ \text{or} \qquad \tan\theta_{\pm(2m-1)} = -1.\end{cases} \qquad (b)
\end{aligned}\tag{27}$$

Within the angular interval $0 < \theta_{\pm(2m-1)} < 2\pi$ the solutions of Eq. (27a) are $\theta_{\pm(2m-1)} = \pi/4$ and $\theta_{\pm(2m-1)} = 5\pi/4$, while the solutions of Eq. (27b) are $\theta_{\pm(2m-1)} = 3\pi/4$ and $\theta_{\pm(2m-1)} = 7\pi/4$. This indicates that, a dark crossed modulation of the amplitude profile is present in all higher diffraction orders of the CGG in Fig. 1, giving the four-leaf clover look to their transverse intensity cross-sections. There is no phase singularity in expression (25). When the phase functions of Eq. (25) and Eq. (26) are compared, it is evident that the $\pm(2m-1)$-th diffraction-order beam, generated by the fork-shaped grating, possess an extra phase expression given by the exponential function $\exp\lfloor \pm i(2m-1)p\theta_{\pm(2m-1)}\rfloor$, which together with the zero amplitude value at $\rho_{\pm(2m-1)} = 0$, declares the beam as a vortex, with topological charge equal to $\pm(2m-1)p$. If we go back to Eq. (25) and use the exponential representation $\cos(2\theta_{\pm(2m-1)}) = \lfloor \exp(i2\theta_{\pm(2m-1)}) + \exp(-i2\theta_{\pm(2m-1)})\rfloor/2$, we come to a conclusion that, the HDOs of the CGG in Fig. 1 represent a sum of two equiaxial vortex beams possessing topological charges +2 and −2. Similar is the situation with the coupling of two oppositely charged Laguerre-Gaussian beams with zero radial modes to obtain an uncharged LG beam

$$\begin{aligned}
U_0^2(\rho,\theta,z) &= A_{0,2}\left(\frac{\sqrt{2}\rho}{w(z)}\right)^2\exp\left(\frac{-\rho^2}{w^2(z)}\right)[\exp(i2\theta)+\exp(-i2\theta)]\\
&= 2A_{0,2}\left(\frac{\sqrt{2}\rho}{w(z)}\right)^2\exp\left(\frac{-\rho^2}{w^2(z)}\right)\cos(2\theta).
\end{aligned}\tag{28}$$

The intensity profiles of the beams Eq. (25) and Eq. (26) are

$$\begin{aligned}
I_{\pm(2m-1)}(\rho_{\pm(2m-1)},\theta_{\pm(2m-1)},z) &= \frac{32}{\pi^3}\frac{1}{(2m-1)^2}\left(\frac{w_0'}{w'(z)}\right)^2\frac{\rho^2_{\pm(2m-1)}}{w'^2(z)}\\
&\times \exp\left[-\frac{2\rho^2_{\pm(2m-1)}}{w'^2(z)}\right]\cos^2(2\theta_{\pm(2m-1)})\\
&\times \left\{I_{(2-1)/2}\left(\frac{\rho^2_{\pm(2m-1)}}{w'^2(z)}\right) - I_{(2+1)/2}\left(\frac{\rho^2_{\pm(2m-1)}}{w'^2(z)}\right)\right\}^2
\end{aligned}\tag{29}$$

for expression (25), and

$$\begin{aligned}
I_{\pm(2m-1)}(\rho_{\pm(2m-1)},z) &= \frac{32}{\pi^3}\frac{1}{(2m-1)^2}\left(\frac{w_0'}{w'(z)}\right)^2\frac{\rho^2_{\pm(2m-1)}}{w'^2(z)}\exp\left[-\frac{2\rho^2_{\pm(2m-1)}}{w'^2(z)}\right]\\
&\times \left\{I_{((2m-1)p-1)/2}\left(\frac{\rho^2_{\pm(2m-1)}}{w'^2(z)}\right) - I_{((2m-1)p+1)/2}\left(\frac{\rho^2_{\pm(2m-1)}}{w'^2(z)}\right)\right\}^2
\end{aligned}\tag{30}$$

for the beam (26).

Based on Eq. (29) the diffraction pattern in the first diffraction order is numerically calculated and presented in Fig. 2, at distances z=0.5 m (a), 1 m (b) and 10 m (c), for parameters $w_0 = 1$ mm and $\lambda = 530$ nm. While in the near field and at distances $z < z_0$ ($z_0 = 5.9$ m) behind the grating, the bright spots are followed with secondary maxima (due to the ringing intensity distribution in radial direction), in the far field they are absent. In Fig. 2d the experimentally registered far-field diffractogram is shown. In the experiment binary CGG produced photolithographically with a grating period of 30 μm, and continuous-wave, frequency-doubled Nd: YVO_4 laser at a wavelength of 532 nm are used. The images are recorded 15 cm out of the artificial far-field in the focus of a lens (f=75 cm) in order to get better resolution of the image with the CCD camera.

In Fig. 3 the presented transverse intensity profiles of the first-diffraction-order beam, at distance z=10 m are calculated on base on Eq. (23), for: l=1 (a), l=1, 2 (b) and l=1, 2, 3 (c). When higher than one values of l are taken in the sum, the central part of the diffraction pattern remains same, but the outer parts of the bright spots are not sharply defined i.e. they are stretched along the crossed directions. It can be seen that Fig. 3.a most closely resembles the experimentally obtained diffractogram.

The radial part of the intensity profile Eq. (29) differs from the intensity profile Eq. (30) in absence of the diffraction-order value $(2m-1)$ in the indices of the modified Bessel functions. The product $(2m-1)p$ is replaced by 2 for all diffraction orders in Eq. (29). In [16] for the doughnut-shaped maximum of the intensity profile Eq. (30), the approximate radius is calculated $(\rho_{\pm(2m-1)})_{\max} = w'(z)\sqrt{\frac{(2m-1)p((2m-1)p+1)}{(2m-1)p+2}}$, which is in good agreement with the lower diffraction orders in experimental checking [23]. If the same approximation is applied in the case of radial part in Eq. (29), we get that the four-leaf clover-profile maxima are on the radii

$$(w_{\pm(2m-1)})_{beam} = w'(z)\sqrt{3/2} \quad \text{and} \quad \theta_{\pm(2m-1)} = 0,\ \pi/2,\ \pi \ \text{and} \ 3\pi/2\ (m = 1, 2, 3, \ldots) \tag{31}$$

in all far-field diffraction orders of the CGG in Fig. 1.

The far-field intensity diffractograms of the CGG (Fig. 1) and of the fork-shaped grating, under Gaussian beam incidence, represent a sum

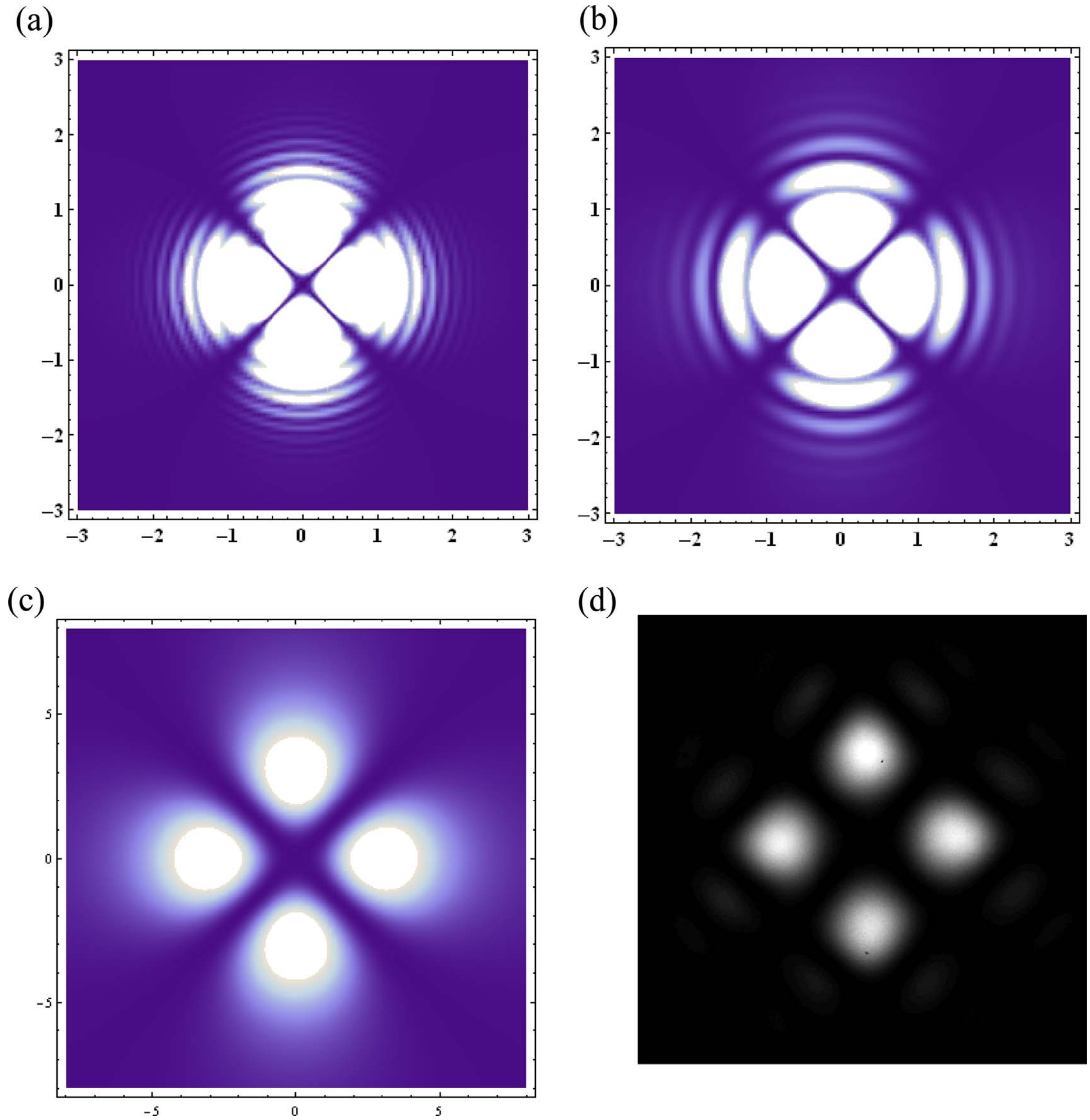

Fig. 2. The calculated difraction patterns of the four-sector grating, in the first diffraction order, a distance z=0.5 m (a), 1 m (b) and 10 m (c), and the experimentally obtained diffraction pattern (d).

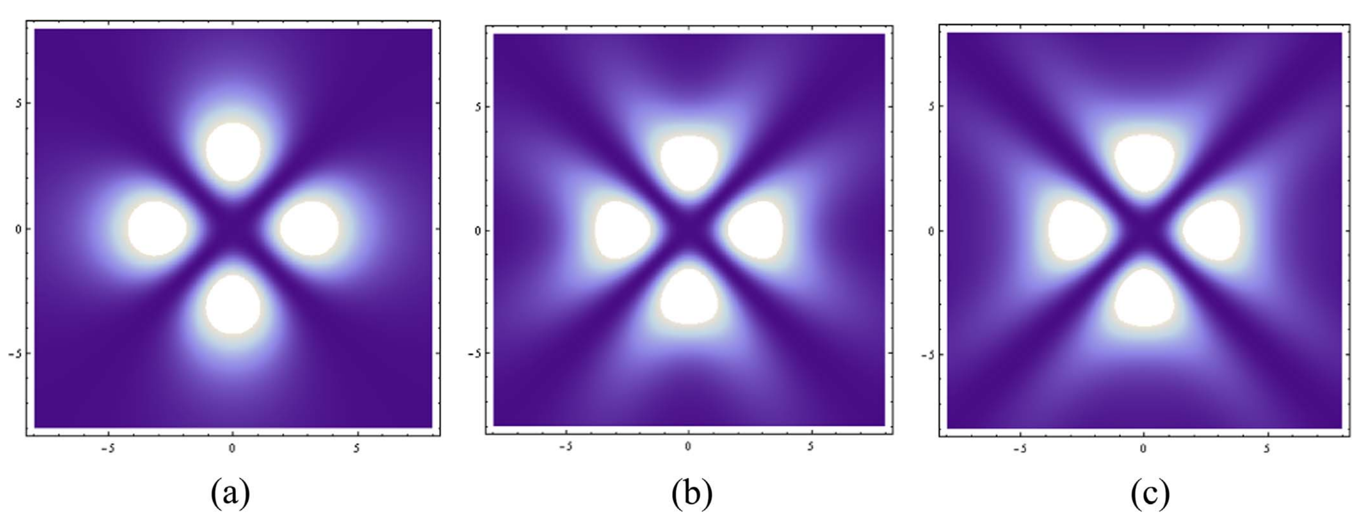

Fig. 3. Transverse intensity profiles of the four-sector grating in the first diffraction order, calculated at distance z=10 m, according Eq. (23) for: l=1 (a), l=1,2 (b) and l=1,2,3 (c).

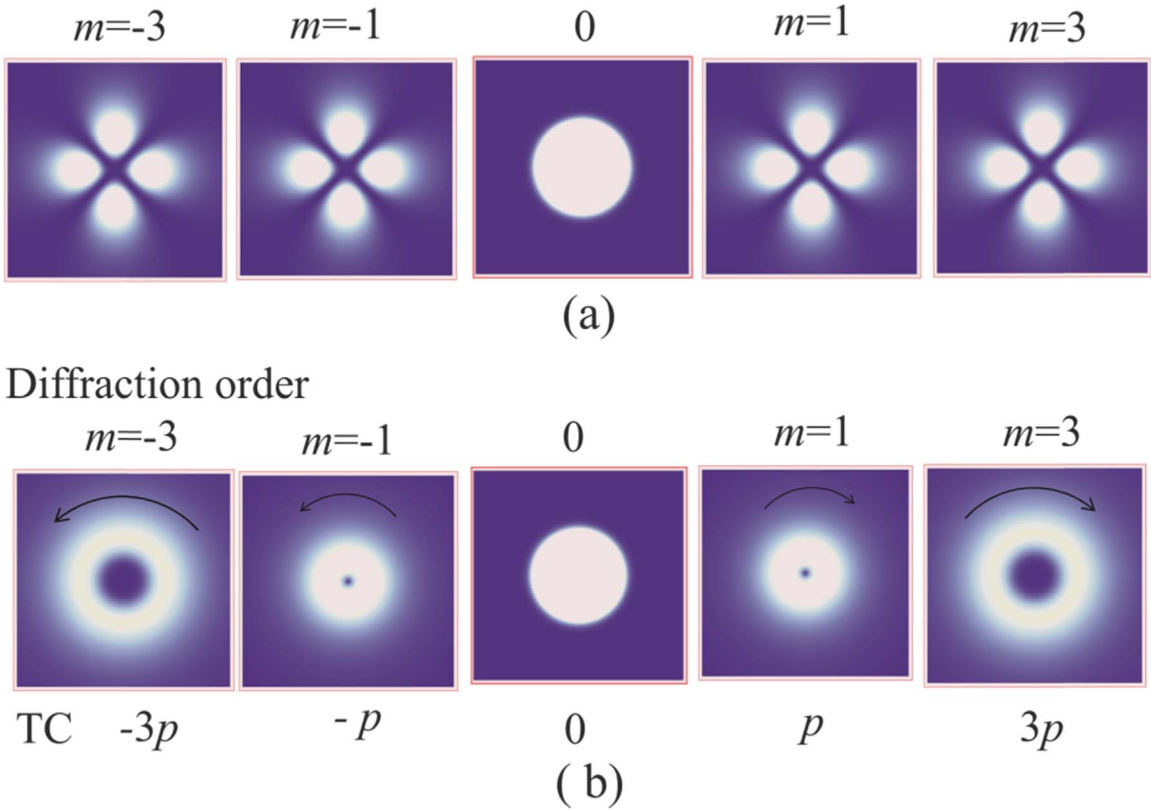

Fig. 4. Diffractograms of the CGGs: a) The diffractogram of the binary four-sector grating (Fig. 1) consists of equisized four-leaf clover-shaped transverse intensity profiles in the higher diffraction orders, and a zeroth-diffraction-order Gaussian beam. b) The diffractogram of the fork-shaped binary grating with p=1 consists of growing in size doughnut-shaped rings in the higher diffraction orders, and a zeroth-diffraction-order Gaussian beam. (The arrows show the direction of rotation of the helicoidal wave fronts).

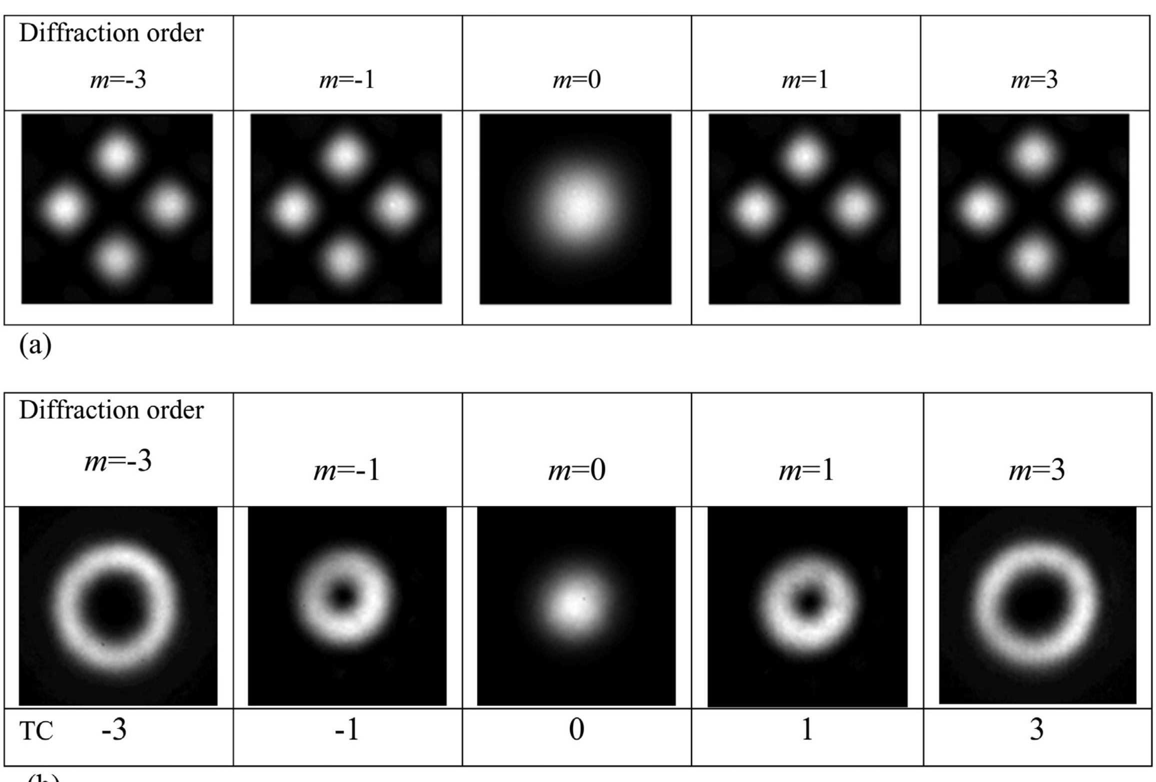

Fig. 5. Experimentally obtained diffraction patterns near the back focal plane of a converging lens, of a binary four-sectorial grating (a), and a fork-shaped grating with p=1 (b).

over all intensity profiles of the separate diffraction-order beam intensities Eq. (29) or Eq. (30). In agreement with the previously discussed theoretical results, it is possible to draw a schematic picture of the expected look of the diffractograms (Fig. 4) - the numerical calculation is done at z=10 m, for parameters $w_0 = 1$ mm and $\lambda = 530$ nm. While, in Fig. 5 the experimentally obtained diffraction patterns of a binary, computer-generated four-sector grating (a) and a fork-shaped grating with topological charge p=1 (b), registered near (15 cm behind) the back focal plane of a converging lens with focal distance f=75 cm are presented.

The statement that the higher diffraction order beams Eq. (25) are not vortices can be supported by their interferograms with a plane wave, tilted by small angle ϑ towards the object beam (Eq. (25)),

$$U = A\exp\left(-i\frac{2\pi}{\lambda}(\sin\vartheta)\rho_{\pm(2m-1)}\cos\theta_{\pm(2m-1)}\right)\exp(-ikz) \quad \text{(where } D' = \lambda/\sin\vartheta\text{)}.$$
$$= A\exp(-i\frac{2\pi}{D'}\rho_{\pm(2m-1)}\cos\theta_{\pm(2m-1)})\exp(-ikz)$$

The equations $F(\rho_{\pm(2m-1)}, \theta_{\pm(2m-1)}) - F_{\pm(2m-1)}(\rho_{\pm(2m-1)}, \theta_{\pm(2m-1)}) = \mu\pi$ ($|\mu| = 0, 1, 2, ...$), where $F = \frac{2\pi}{D'}\rho_{\pm(2m-1)}\cos\theta_{\pm(2m-1)} + kz = \frac{2\pi}{D'}x_{\pm(2m-1)} + kz$ is a phase function of a plane wave front defined in polar coordinate system with centre in $O_{\pm(2m-1)}$, and $F_{\pm(2m-1)}$ are the phase functions of the beams Eq. (25), define the interference fringes. So, in the far-field approximation, and taking the interferogram plane to be z=constant, the fringe pattern is defined by equations: $x_{\pm(2m-1)} = \frac{(2m-1)^2\lambda z/(8\xi_0^2) - \mu/2}{-1/D' \mp (2m-1)/(2\zeta_0)}$. It is a system of straight lines, normal to the polar axis of the local coordinate system. They are modulated by the intensity background $A^2 + I_{\pm(2m-1)}(\rho_{\pm(2m-1)}, \theta_{\pm(2m-1)}, z)$, as it is seen in Fig. 6: numerically

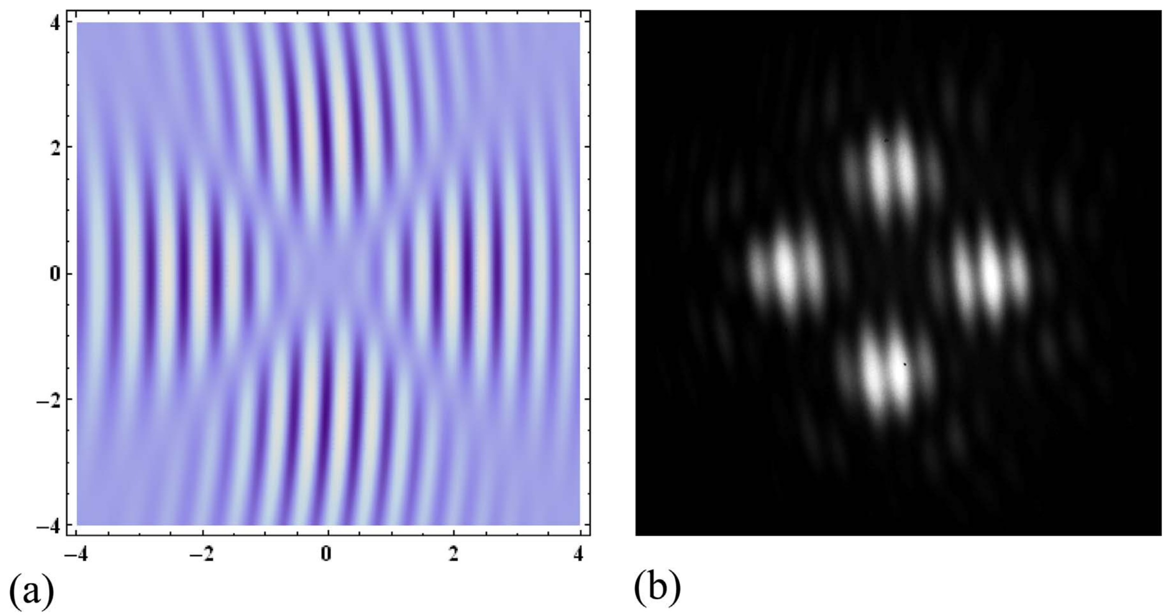

Fig. 6. Interference pattern of the beam shown in Fig. 2.c with an inclined plane wave: numerically calculated (a) and experimentally obtained (b).

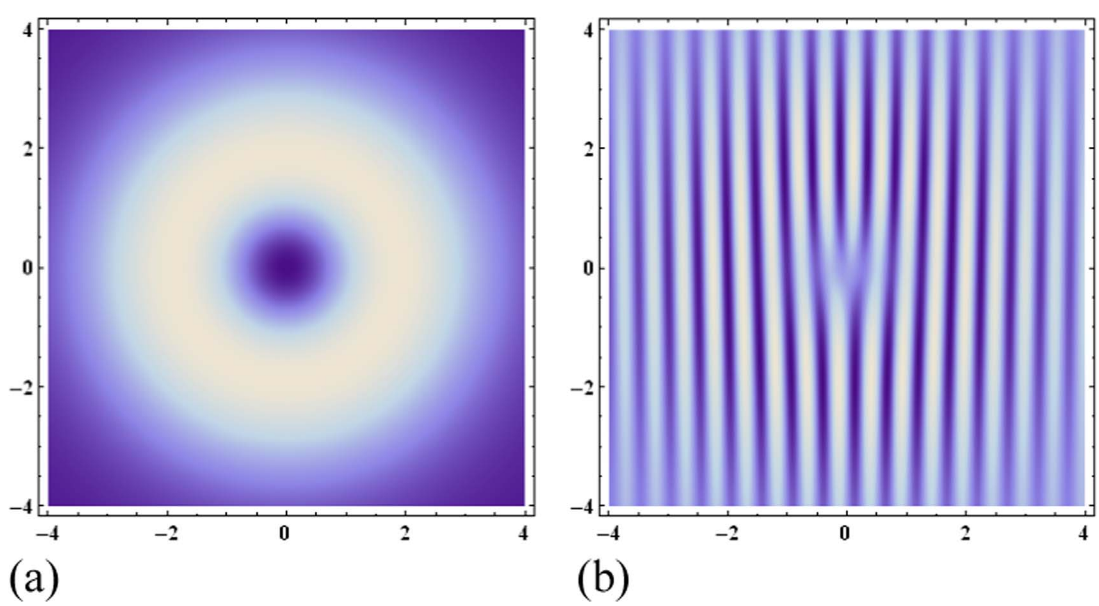

Fig. 7. Vortex beam obtained with the fork-shaped grating (a) and its interference pattern with inclined plane wave (b), for m=1, p=1 and z=10 m.

calculated (a) and experimentally obtained (b) pattern. In Fig. 6.a the following parameters are used: A=1, m=1, z=10 m, $w_0 = 1$ mm and $\lambda = 530$ nm (as in the rest of the numerical calculations). If the interference of the tilted plane wave occurred with one of the beams Eq. (26), the fringe pattern is defined by $\frac{2\pi}{D'}x_{\pm(2m-1)} \mp mp\theta = \mu\pi$, showing that is a fork-shaped pattern over the intensity background $A^2 + I_{\pm(2m-1)}(\rho_{\pm(2m-1)}, z)$ with the doughnut ring around the fork-shaped part, as a modulator (Fig. 7.b). In the computer calculation of Fig. 7 we have set: A=1, m=1, p=1 and z=10 m.

5. Conclusion

In this article we investigated a computer-generated grating composed by parts of a binary rectilinear grating nested into four equal angular sectors, bounded by the directions $y = x$ and $y = -x$, along which each two neighboring parts are shifted by a half spatial grating period. Through the analytical method we have derived the wave field amplitude and intensity distribution in the observation plane behind the grating, in the process of Fresnel diffraction of an incident Gaussian beam. The far-field diffraction pattern was numerically and experimentally obtained. While the zeroth-diffraction-order beam is ordinary Gaussian, the odd HDOs are found as equal in size X-modulated beams; They look similar to the linear combination of two LG modes with radial mode number equal to zero, and opposite azimuthal mode numbers +2 and −2, or as HG(1,1) mode. Thus, this type of CGG can be used as a substitute to the laser resonator in order to produce four-leaf clover-shaped intensity profile with chargeless central dark spot. It can be used for precise angular alignment, in optical trapping, where the azimuthally nested bright spots can be used as separate traps for particles with higher refractive index than the surrounding medium, and in fiber optics for transfer of information. The studies of the escape and synchronization of a particle between two adjacent bright spots, acting as optical traps in azimuthal direction, could be of interest in statistical physics research, similarly as the intensity profile obtained by optical elements constructed as phase layers with cosine-profiled periodicity in the azimuthal direction [24] can be used for.

Acknowledgments

L.S. and A.D. acknowledge funding of the National Science Fund (Bulgaria) within the framework of Project DFNI-T02/10–2014.

References

[1] H. Kogelnik, T. Li, Laser beams and resonators, Appl. Opt. 5 (1966) 1550–1567.
[2] Y. Cai, C. Chen, Paraxial propagation of a partially coherent Hermite-Gaussian beam through aligned and misaligned *ABCD* optical systems, J. Opt. Soc. Am. A 24 (2007) 2394–2401.
[3] L. Allen, S.M. Barnett, M.J. Padgett, Optical Angular Momentum, Institute of Physics Publishing, Bristol, 2003.
[4] J.F. Nye, M.V. Berry, Dislocations in wave trains, Proc. R. Soc. Lond. A. 336 (1974) 165–190.
[5] I.V. Basistiy, M.S. Soskin, M.V. Vasnetsov, Optical wavefront dislocations and their properties, Opt. Commun. 119 (1995) 604–612.
[6] S.N. Khonina, V.V. Kotlyar, M.V. Shinkaryev, V.A. Soifer, G.V. Uspleniev, The phase rotor filter, J. Mod. Opt. 39 (1992) 1147–1154.
[7] M.W. Beijersbergen, R.P.C. Coerwinkel, M. Kristensen, J.P. Woerdman, Helical-wavefront laser beams produced with a spiral phase plate, Opt. Commun. 112 (1994) 321–327.
[8] V.V. Kotlyar, A.A. Almazov, S.N. Khonina, V.A. Soifer, H. Elfstrom, J. Turunen, Generation of phase singularity through diffracting a plane or Gaussian beam by a spiral phase plate, J. Opt. Soc. Am. A 22 (2005) 849–861.
[9] S.N. Khonina, V.V. Kotlyar, V.A. Soifer, M.V. Shinkaryev, G.V. Uspleniev, Trochoson, Opt. Commun. 91 (1992) 158–162.
[10] V.V. Kotlyar, A.A. Kovalev, R.V. Skidanov, O. Yu Moiseev, V.A. Soifer, Diffraction of a finite-radius plane wave and a Gaussian beam by a helical axicon and a spiral phase plate, J. Opt. Soc. Am. A 24 (2007) 1955–1964.
[11] J.A. Davis, E. Carcole, D.M. Cottrell, Intensity and phase measurements of nondiffracting beams generated with a magneto-optic spatial light modulator, Appl. Opt. 35 (1996) 593–598.
[12] S. Topuzoski, Lj Janicijevic, Conversion of high order Laguerre-Gaussian beams into Bessel beams of increased, reduced or zero-th order by use of a helical axicon, Opt. Commun. 282 (2009) 3426–3432.
[13] Lj Janicijevic, S. Topuzoski, Gaussian laser beam transformation into an optical vortex beam by helical lens, J. Mod. Opt. 63 (2016) 164–176.
[14] A. Vasara, J. Turunen, A.T. Friberg, Realization of general nondiffracting beams with computer-generated holograms, J. Opt. Soc. Am. A 6 (1989) 1748–1754.
[15] N.R. Heckenberg, R. McDuff, C.P. Smith, A.G. White, Generation of optical phase singularities by computer-generated holograms, Opt. Lett. 17 (1992) 221–223.
[16] Lj Janicijevic, S. Topuzoski, Fresnel and Fraunhofer diffraction of a Gaussian laser beam by fork-shaped gratings, J. Opt. Soc. Am. A 25 (2008) 2659–2669.
[17] A. Bekshaev, O. Orlinska, M. Vasnetsov, Optical vortex generation with a “fork” hologram under conditions of high-angle diffraction, Opt. Commun. 283 (2010) 2006–2016.
[18] S.N. Khonina, V.V. Kotlyar, V.A. Soifer, K. Jefimovs, J. Turunen, Generation and selection of laser beams represented by a superposition of two angular harmonics, J. Mod. Opt. 51 (2004) 761–773.
[19] M. Abramowitz, I.A. Stegun, Handbook of Mathematical Functions, Dover publ. Inc., New York, 1964.
[20] H. Bateman, A. Erdelyi, Higher Transcendental Functions II, Nauka, Moscow, 1974.
[21] A.P. Prudnikov, Y.A. Brichkov, O. Marichev, Integrals and series, special functions, Science, Moscow, 1983.
[22] Z.S. Sacks, D. Rozas, G.A. Swartzlander, Holographic formation of optical-vortex filaments, J. Opt. Soc. Am. B 15 (1998) 2226–2234.
[23] L. Stoyanov, S. Topuzoski, I. Stefanov, Lj Janicijevic, A. Dreischuh, Far field diffraction of an optical vortex beam by a fork-shaped grating, Opt. Commun. 350 (2015) 301–308.
[24] S. Topuzoski, Lj Janicijevic, Diffraction characteristics of optical elements designed as phase layers with cosine-profiled periodicity in the azimuthal direction, J. Opt. Soc. Am. A 28 (2011) 2465–2472.